Nonmonotonic Size-Dependent Carrier Mobility in PbSe Nanocrystal Arrays

ARTICLE *in* JOURNAL OF PHYSICAL CHEMISTRY LETTERS · MARCH 2012

Impact Factor: 7.46 · DOI: 10.1021/jz300035t

3 AUTHORS, INCLUDING:

Eunji Sim
Yonsei University
62 PUBLICATIONS **847** CITATIONS

SEE PROFILE

THE JOURNAL OF PHYSICAL CHEMISTRY Letters

Letter

pubs.acs.org/JPCL

Nonmonotonic Size-Dependent Carrier Mobility in PbSe Nanocrystal Arrays

Jihye Lee, One Choi, and Eunji Sim*

Department of Chemistry and Institute of Nano-Bio Molecular Assemblies, Yonsei University, 50 Yonsei-ro Seodaemun-gu, Seoul 120-749, Korea

ABSTRACT: On the basis of a tight binding system-bath model, we investigated carrier mobility of PbSe nanocrystal (NC) arrays as a function of NC size and inter-NC separation. The size-dependent trend of calculated carrier mobilities are in excellent agreement with recent experimental measurements: electron mobility increased up to NC diameter of ~6 nm and then decreased for larger NCs, whereas hole mobility showed a monotonic size-dependency. Carrier mobility increase was associated with reduced activation energy that governs charge-transfer processes. In contrast, the decrease in electron mobility for large NCs was found to be due to smaller electronic coupling. Control of inter-NC separation is crucial for mobility enhancement: the mobility may change by an order of magnitude when inter-NC separation varies by as little as 1 to 2 Å. We anticipate similar size-dependency of the mobility in other semiconductor NC arrays, although crossover diameter in which mobility reaches its maximum depends on the material.

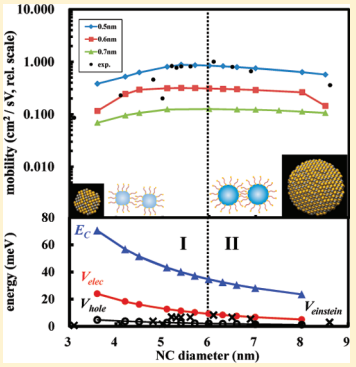

SECTION: Electron Transport, Optical and Electronic Devices, Hard Matter

On account of recent development in granular electronic material for potential applications in electronic and optoelectronic devices, it has become critical to understand electronic properties of colloidal semiconductor nanocrystals (NCs). In particular, the majority of semiconductor nanoscience is focused on the formation of NC arrays and understanding of the transport and optical properties of these arrays.[1] At room temperature, mobility of electron or hole carriers in semiconductor NC arrays was reported to increase with NC size.[2,3] Electron mobility of CdSe NC arrays was observed to increase as NC grows in size from 3 to 5 nm.[2] Hole mobility of PbSe NCs also exhibited a similar trend of monotonic increase in the range of 3.1−8 nm NC diameter. What is more interesting about PbSe NCs is that electron mobility increases by one to two orders of magnitude as the NC size changes from 3.1 to 6 nm, and then it decreases for larger NCs.[3] Clearly the mobility is an outcome of complex interplay of numerous factors. In general, a smaller number of hops that are required for electronic transport or a systematic decrease in the activation energy and the depth of trap states have been speculated as being responsible for the mobility increase with NC size.[2,3] Nevertheless, the decrease in electron mobility for larger PbSe NCs could not be explained. The number of hopping decreases by only a factor of 2 as the NC size doubles: its effect is insufficient to explain the mobility enhancement over 10 times. Activation energy and carrier mobility are related to an Arrhenius type behavior, $\mu = \mu_0 \exp(-E_A/k_BT)$.[4] It is known that the activation energy decreases with NC size which, in turn, promotes carrier mobility.[2] However, the electron mobility decrease for large PbSe NC arrays is not supported by the activation energy decrease.

According to the Einstein−Smoluchowski equation,[5] carrier mobility (μ) and electronic coupling between neighboring NCs (V) has the relationship of $\mu = (e/2hk_BT)s^2V$, where e, h, k_B, T, and s, respectively, are electron charge, Planck constant, Boltzmann constant, temperature, and internanocrystal (inter-NC) separation. Assuming a uniform distribution of NCs with a fixed inter-NC separation, the Einstein relation states that the mobility should depend solely on the electronic coupling. In other words, the size-dependent character of μ should coincide with that of V. The electronic coupling obviously shows a monotonic trend with NC size, and thus the nonmonotonic trend of electron mobility is inconsistent with the Einstein−Smoluchowski relation. Determination of the electronic coupling is not a simple matter: properties of NC particles (size, shape, charge trapping states, surface defects, etc.) along with those of ligand molecules (length, dielectric constant, linking ability, etc.) should all be taken into consideration comprehensively. On the basis of the report that the influence of NC size disorder on the carrier mobility is insignificant,[3] we have ignored energy distribution associated with size and shape disorder as well as surface defects, although control of the form of disorder/defects is important for improving electronic transport in semiconductor NC arrays. In this Letter, we explore and determine the factors that govern the nonmonotonic size-dependent mobility by focusing on the electronic coupling and the charging energy along with inter-NC separation.

Received: January 10, 2012
Accepted: February 22, 2012

   dx.doi.org/10.1021/jz300035t | J. Phys. Chem. Lett. 2012, 3, 714−719

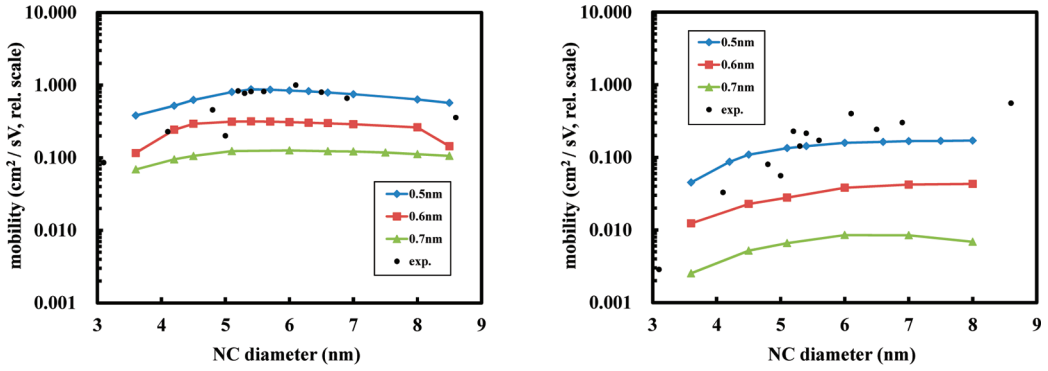

Figure 1. Electron and hole mobility of PbSe nanocrystal arrays. Experimental data are taken from ref 3, table 1. Each marker represents the corresponding inter-NC separation (s) model data, whereas solid lines are drawn for guidance. Both experimental and computed carrier mobilities are in $cm^2\ V^{-1}\ s^{-1}$ unit and renormalized for comparison.

Figure 1 compares computed electron and hole mobilities of PbSe NC arrays with experimental data as a function of NC size. Time evolution of the carrier population on NCs was obtained by the on-the-fly filtered propagator functional path integral (OFPF-PI) method.[6−11] The computed electron and hole mobilities agree excellently with the experimental observation without employing any size-dependent adjustable parameter. With respect to the NC size, nonmonotonic behavior of the electron mobility (Figure 1a) and monotonic increase in the hole mobility (Figure 1b) are clearly visible. In particular, the experimental electron mobility agrees well with the computed counterparts of s = 0.5 nm, which is the length of ethane dithiol ligand.[12] For a given inter-NC separation, however, the crossover diameter where electron mobility reaches its maximum varies. In the following, we discuss the model system used to reproduce the experiment presented in Figure 1.

The PbSe NC electronic transport system was modeled as a 1-D five-state tight-binding charge transfer system coupled to a harmonic bath with the following Hamiltonian[13,14]

$$H = \Delta E \sum_{k=1}^{5} k|k\rangle\langle k| + \sum_{k=1}^{5} V\{|k\rangle\langle k \pm 1|\} + \sum_{n=1}^{Q} \left\{ \frac{1}{2} M_n \dot{x}_n^2 + \frac{1}{2} M_n \omega_n^2 x_n^2 \right\} - \sum_{n=1}^{Q} c_n x_n \sum_{k=1}^{5} |k\rangle\langle k| \quad (1)$$

where $|k\rangle$ represents the electronic state in which the carrier populates the kth NC without invoking complex electronic structures of PbSe NC arrays. For instance, $|3\rangle$ represents $P_1 - P_2 - P_3^* - P_4 - P_5$, where P_m denotes the mth NC that is neutral, whereas P_3^* is the charged one. x_n is the nth bath mode that is coupled to the system by the coupling strength c_n. Recently, single-electron tunneling spectra for PbSe NCs have shown strong coupling between carriers and longitudinal-optic phonon modes.[15] This supports the modeling dissipative environment as harmonic oscillators in eq 1. These oscillators correspond to the phonon modes of a solid, although there are other situations where a harmonic bath description is relevant by virtue of a linear response approximation. Because of the long-range nature of the Coulomb potential, a large number of phonon modes are involved, and the role of the medium is equivalent to that of a Gaussian heat bath.[6,16,17] Despite its simple form, system-bath Hamiltonian with bilinearly coupled harmonic bath model has long proven to provide successful description for various quantum dynamics such as charge-transfer processes in reaction centers,[18,19] DNA,[20−22] and molecular wires.[23] The chosen five-state tight-binding system is too small to represent the micrometer scale of NC array samples. Nevertheless, essential dynamics of charge transfer can be well-represented by using more than three electronic states.

The charge-transfer dynamics of the system described by eq 1 is explored through time-evolution of the reduced density matrix, $\tilde{\rho}(t) = Tr_b[e^{-iHt/\hbar}\rho(0)e^{iHt/\hbar}]$, where Tr_b denotes the trace of all bath degrees of freedom. $\rho(0)$ describes the thermally equilibrated initial condition and $e^{-iHt/\hbar}(e^{iHt/\hbar})$ is the forward(backward) propagator. Computation of the density matrix of a quantum system is often a formidable task owing to the exponential growth of computation amount with time and the system size as M^{2N} at $t = N\Delta t$, where M is the number of states and Δt is the integration time step. However, use of the OFPF-PI method along with harmonic bath model allows efficient on-the-fly sorting of significantly contributing pair trajectories out of an almost infinite number of trajectories; therefore, computation of relatively long-time dynamics can be performed on a practical time scale.[8,9,11,24−27] Details of the OFPF-PI method can be found elsewhere.[10,11,27]

By definition, carrier mobility is $\mu = v/E$, where v is the drift velocity and E is the applied external field.[28] Although the drift velocity should depend on the applied electric field, the carrier mobility takes a constant value under a low electric field. Suppose that the charge-transfer rate is k for a NC array in which center-to-center distance between neighboring NCs is $D = d + s$, sum of NC diameter and inter-NC separation. Using the connection between the drift velocity and the charge transfer rate, $v = Dk$, and also the relation of the external field to the energy difference between neighboring NCs (ΔE), $E = \Delta E/D$, the mobility can be rewritten as $\mu = kD^2/\Delta E$ with the unit of $cm^2\ V^{-1}\ s^{-1}$. From the time-evolution of the carrier population, that is, diagonal elements of the reduced density matrix, the charge-transfer rate constant can readily be extracted. By assuming an exponential decay (−) or rise (+) of the carrier population in the case of the nearest-neighbor hopping mechanism, $\tilde{\rho}(t) = \tilde{\rho}(0)\exp(\pm kt)$ fit can be used.

dx.doi.org/10.1021/jz300035t | J. Phys. Chem. Lett. 2012, 3, 714−719

To explore the origin of the nonmonotonic electron mobility, let us discuss the parameters used to model PbSe NC arrays. We ignored energy distribution due to the size and shape disorder as well as the surface defects of NCs; therefore, the energy difference between neighboring NCs is equal to the applied bias voltage between them and is set to be 10 meV.[3] Different choices of ΔE produced no visible difference in computed carrier mobilities as long as the electric field is low. The site energy disorder in this model is provided by the applied electric field, which, along with thermal heat bath, invokes charge transfer from state $|1\rangle$ to $|5\rangle$. The electronic coupling was estimated using a double quantum-well model along with the effective mass approximation. The approximation allows calculating the transmissivity of a multiple quantum-well system in Kronig–Penney model; thereby splitting of resonant peak energy can be obtained.[29] The electronic coupling strength is then estimated to be one-half of the splitting of the two lowest energy states of the corresponding double quantum-well system. The increased electronic coupling leads to larger splitting of the resonant energy. The electron and hole effective mass of PbSe NCs and the electron effective mass of aliphatic ligand were taken from the literature.[30,31] The hole effective mass of ethane dithiol ($m^*_{b,h}$) was arbitrarily chosen as long as it was greater than the electron effective mass accommodating the lower hole mobility than the electron mobility. Such arbitrary choice of $m^*_{b,h}$ may explain relatively poor agreement of the hole mobility in Figure 1b.

Strength of the electronic coupling between NCs depends in large part on the capping molecule. The barrier width (inter-NC separation)[32,33] and (tunnel) barrier height in Scheme 1 greatly affect the electronic coupling. Exchanging long-chain organic ligands with short ones increases electronic coupling owing to the decreased barrier width.[34] Replacing saturated ligands with either conjugated ones[35] or an inorganic material[36] of lower effective mass improves electronic coupling by reducing the barrier height. Liu et al. performed experiments with various alkane dithiol ligands: from ethane dithiol to hexane dithiol. In this work, ethane dithiol ligand was modeled with corresponding dielectric constant (ε_r = 2.7)[37] and barrier height (E_b = 2 eV).[38] In comparison, the dielectric constant for bulk PbSe is very high ($\varepsilon \sim 250$) and $\varepsilon > 100$ was measured for individual 12 nm PbSe NCs.[39] Use of a longer alkane chain leads to a larger spacing and gives rise to the reduction of electronic coupling which, in turn, lower carrier mobility. The authors noted that NC arrays were rather glassy as opposed to the crystal lattice in the sense that the inter-NC separation as well as NC size and shape distribution could not be perfectly regulated.[3] Therefore, we selected model systems with a range of inter-NC separations for assessing the effects. For both electron and hole mobilities, models of s = 0.5, 0.6, and 0.7 nm were studied after considering the dimension of ethane dithiol (~0.5 nm). The carrier mobility indeed decreased exponentially with the inter-NC separation.[3] Parameters used for the double quantum-well model are listed in Table 1. A monotonic decrease in the electronic coupling was obtained from the double quantum-well model. Smaller electronic coupling deteriorates carrier mobility as a NC becomes larger. Obviously the increasing trend of both electron and hole mobilities does not develop from the electronic coupling.

Scheme 1. One-Dimensional Double Quantum-Well Structure Used for Electronic Coupling Calculations

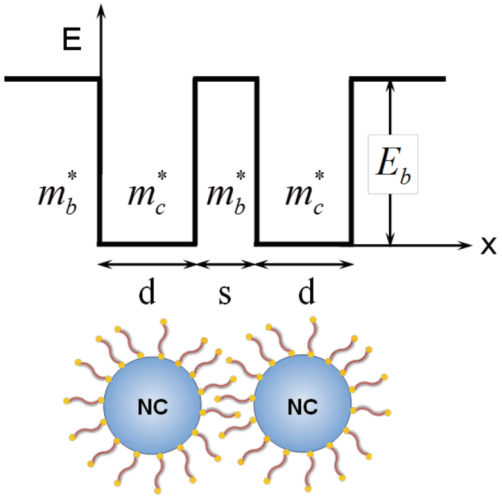

Table 1. Potential Parameters Used for PbSe Nanocrystal Array Model[a]

m_e^*	m_h^*	$m_{b,e}^*$	$m_{b,h}^*$	E_b (eV)	ε_r	ΔE (meV)
0.05	0.05	0.28	0.82	2.0	2.7	10

[a]Electron (m_e^*) and hole (m_h^*) effective mass of PbSe NCs, electron ($m_{b,e}^*$) and hole ($m_{b,h}^*$) effective mass of aliphatic ligand, barrier height (E_b), relative dielectric constant (ε_r) of ligand, and energy bias between neighboring PbSe nanocrystals (ΔE).

By using effective mass approximation with the double quantum-well model, detailed electronic structure of PbSe is not explicit, whereas its complex band structure affects carrier mobility of PbSe NC arrays. Because all NCs are identical, coupling between equivalent bands of neighboring NCs should be the strongest. Therefore, we assumed that the overall electronic coupling for a carrier is mainly determined by the coupling between corresponding electronic states/bands, which are the most responsible for the carrier transfer: the conduction band plays an important role for the electron transfer, whereas the valence band is involved in the hole transfer. Therefore, in eq 1, without getting into detailed PbSe electronic structure, we describe coupling between relevant electronic states. Solving the Schrödinger equation for the double quantum-well (Scheme 1) for the two lowest energy levels results in the hybridization of the lowest equivalent band levels of the isolated PbSe quantum dots. If the particle of interest is an electron, then two lowest conduction band splittings are obtained, whereas the two lowest valence band levels are obtained for a hole. In other words, eq 1 is equivalent to considering the conduction (valence) band only for the electron (hole) transfer.

Next, we consider the reorganization energy in conjunction with the charge-transfer activation energy. Because the bath in eq 1 consists of semi-infinite number of bath modes, it is advantageous to utilize the spectral density instead of treating bath modes explicitly. For harmonic bath modes, the spectral density can be defined as[7,40]

$$J(\omega) = \frac{\pi}{2}\sum_{n=1}^{Q}\frac{c_n^2}{m_n\omega_n}\delta(\omega - \omega_n) \qquad (2)$$

dx.doi.org/10.1021/jz300035t | J. Phys. Chem. Lett. 2012, 3, 714–719

Here we employed Ohmic spectral density with the characteristic cutoff frequency ω_c and the reorganization energy λ as follows[41]

$$J(\omega) = \pi\lambda\frac{\omega}{\omega_c}\exp(-\omega/\omega_c) \quad (3)$$

Charge-transfer activation energy is the sum of size-dependent Coulomb penalty and inherent energy disorder due to particle size distribution.[42,43] Semiconductor NCs have a size-dependent charging energy that is required to transfer a single charge to a neutral NC.[44] When the size and shape disorder is ignored, it is reasonable to assume that the charge-transfer activation energy is equal to the charging energy (E_C).[42] Then, the reorganization energy can be determined from the tight-binding potential energy surfaces.[16] As NC diameter increases, the charging energy is reduced as the following equation: the array charging energy is the inverse of the sum of current carrying NC capacitances (C_{nn}) as[44,45]

$$E_C = \frac{1}{\beta C_{nn}} = \frac{e^2}{\beta 2\pi\varepsilon_0\varepsilon_r d\ \ln(1 + d/s)} \quad (4)$$

where β is the number of current carrying nearest NCs ($2 \leq \beta \leq 12$) and ε_0 is the vacuum permittivity. Among different values of β that have been computed, the model with $\beta = 2$ successfully explained the experimental findings. Models with $\beta = 6$ were examined for which all six nearest-neighbor NCs in 2D array are taken into account; however, the electron mobility monotonically decreased from 3 to 8 nm in NC size. A recent report on NC arrays found that $\beta = 9$ for eq 4 provided an optimum fitting curve to experimental values.[44] Computed results on our models with $\beta = 9$ did not agree well with the PbSe NC experiment. Again, the electron mobility decreased monotonically. Therefore, we believe that the agreement of $\beta = 2$ models indicates that two nearest NCs carry most of the current in the percolation network of the charge transfer in these NC arrays.

At this point, let us examine the nonmonotonic behavior of the electron mobility. Figure 2 compares the charging energy from eq 4 and the electronic coupling from the double quantum-well model as a function of NC size. Clearly, both the charging energy and the electronic coupling decrease with growing NCs. To distinguish the two regimes of interest with respect to the trend of electron mobility, a dotted line is inserted at 6 nm: **I** on the left indicates the regime where NC diameter is $d \leq 6$ nm, whereas **II** on the right denotes the regime where $d > 6$ nm. In the regime **I**, electron mobility shows a monotonic increase, whereas it decreases in the regime **II**. The charging energy, that is, the charge-transfer activation energy, decreases rather drastically in the regime **I**, causing the mobility to increase. The decreasing rate of the activation energy, however, also diminishes with NC size, and thus the change becomes relatively little in the regime **II**. In contrast with the charging energy, the smaller electronic coupling further inhibits current flow as NC becomes larger. In regime **II**, the activation energy is already too low that additional reduction provides little improvement in the carrier mobility. Therefore, we believe that the decrease in carrier mobility in large NC arrays is mainly due to severe weakening of the electronic coupling. In other words, the size-dependency of charging energy and electronic coupling conflicts with each other. In consequence, the competition between the two factors determines the overall size-dependency: carrier mobility increases where low activation energy dominates and decreases with weak electronic coupling. For the hole mobility, however, the electronic coupling is relatively weaker than that for the electron mobility; thereby the activation energy governs the charge-transfer process for the whole NC diameter range considered in this work. As shown in Figure 2, the electronic coupling that reproduces the experimental electron mobility according to the Einstein−Smoluchowski relation agrees well with that obtained from the quantum-well model in the regime **II**. In the regime **I**, the Einstein−Smoluchowski relation stipulates stronger electronic coupling with NC size, which is contradictory. Note that the Einstein−Smoluchowski relation ignores the role of charging energy. Therefore, the agreement of electronic couplings in the regime **II** can be considered as supporting information that the charge transfer is indeed governed by the electronic coupling. In fact, we have tried to determine the relationship between charging energy and electronic coupling with which characteristic crossover diameter is defined. So far, we have been unable to find a simple rule that relates the two parameters. As expected, boundary between the two regimes is determined not only by the two parameters but also by the energy difference and reorganization energy.

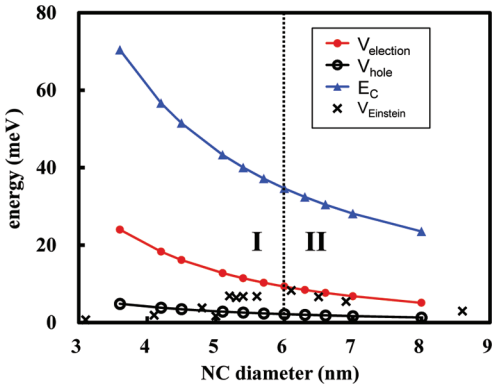

Figure 2. Size-dependent charging energy along with electronic coupling at a given inter-NC separation ($s = 0.5$ nm). Dotted line at 6 nm is drawn to divide the two regimes of interest according to electron mobility trend: **I** on the left indicates the regime where NC diameter $d \leq 6$ nm, whereas **II** on the right denotes the regime, where $d > 6$ nm. X markers denote the electronic coupling for electron transfer that are required to reproduce the experimental electron mobility of ref 3 according to Einstein−Smoluchowski relation.

Regarding the electron mobility at $d \leq 5$ nm, the experimental electron mobility is lower than what is calculated with $s = 0.5$ nm. Near 3 nm NC diameter, in fact, the experimental electron mobility is rather close to the calculated value at $s = 0.6$ nm. The electron mobility when NC diameter is 3−5 nm lies between the results calculated at $s = 0.5$ and 0.6 nm. The inter-NC separation in the experimental system appears to be longer for smaller NC particles and shorter for larger NCs. This may reflect the ligand arrangement on the NC surface. The space filling model of PbSe NC in Figure 3 illustrates that the surface of NC is mostly faceted when NC is small and becomes rounder (a smaller fraction of the surface is faceted) as the size of NCs increases. As schematically drawn in Figure 3, on a faceted surface, ligand molecules are aligned to be rather denser than those on a curved surface. Dense ligand arrangement on small NC particles prevents ligand penetration and leads to a large inter-NC separation. On a round surface, however, ligands may stretch out and leave a space between

dx.doi.org/10.1021/jz300035t | J. Phys. Chem. Lett. 2012, 3, 714−719

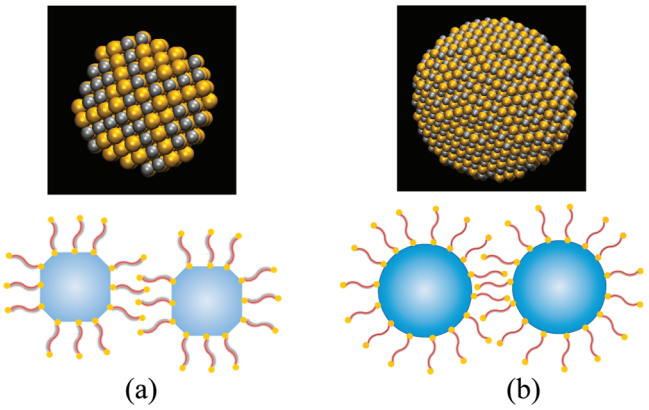

Figure 3. Space-filling model of PbSe nanocrystal on the top and schematic drawings of ligand arrangement at the bottom for (a) 3 and (b) 6 nm diameter. Yellow and gray beads represent Se and Pb atoms, respectively. Surface relaxation is ignored in the space filling model of PbSe nanocrystals.

neighboring ligands. This allows ligands from the adjacent NCs to penetrate the capped layer. Consequently, large NC particles can be packed in a tight configuration, and the inter-NC separation becomes as close as the ligand length. Recently dissipative particle dynamics method was used to show that spherical nanoparticles are coated spontaneously with highly asymmetric ligand arrangements, affecting the structures of aggregated nanoparticles.[46] Also, a recent study reported that van der Waals interaction between NC particles increases with NC size and leads to shorter inter-NC separation for larger NC particles.[47]

For small NCs in Figure 3, electronic coupling between nearest NCs can also be significantly affected by the respective facet orientation of the NCs. In experiments, the distance between two electrodes is too long compared with the dimension of the NCs considered. Therefore, a carrier has to make a number of hops before it reaches the electrode. In other words, the effects of electronic coupling disorder due to respective facet orientation of NCs are averaged during the long-distance travel through random configuration of the glassy system. This was manifested in the experiment that size, shape, and local geometry disorder had little influence on the overall trend of the carrier mobility.[3]

One cannot rule out the possibility of nonmonotonic behavior from the change in the charge-transfer mechanism. Previously, we have shown that the biexponential behavior of DNA hole-transfer rate accounts for the mechanism change from fully coherent hole transfer through a couple of Adenine bridges to variable range hopping mechanism for longer sequences.[21] The charge-transfer mechanism can be determined on a quantitative basis by performing the OFPF-PI in combination with the reduced trajectory space convergence scheme.[27] Upon search for the smallest reduced pair trajectory space that produces the convergent dynamics, one can estimate the coherence length (CL) of a system that is crucial to determine the charge-transfer mechanism:[27] $CL = 2$ indicates the nearest neighbor hopping mechanism, whereas $CL = M$ corresponds to the fully coherent (possibly superexchange) mechanism. $2 < CL < M$ means the through-bridge hopping or variable range hopping mechanism in which a part of the system is strongly coherent.[26] It was found that the nearest-neighbor hopping mechanism governs the charge transfer in PbSe NC arrays for the entire range of the NC size. When models with $\beta = 9$ were examined with the path integral computation, we observed the charge-transfer mechanism shift from nearest-neighbor hopping to the through-bridge (variable range) hopping. However, the model could not explain the experimentally observed trend, not even qualitatively. All $\beta = 2$ models resulted in the nearest-neighbor hopping mechanism. This indicates that the nonmonotonic behavior of the electron mobility is not caused by the change in the charge-transfer mechanism.

In this Letter, we investigated the nonmonotonic electron mobility trend in PbSe NC arrays. The parameters are adapted from the double quantum-well model with effective masses and the array charging energy model. The time-dependent density matrix of a tight binding system-bath Hamiltonian was evaluated using the path integral method. Because the size-dependent effect of the charging energy is the opposite to that of the electronic coupling, relative strength of the two factors determines the size-dependency of carrier mobility. When an NC is small, the low charging energy enhances the carrier mobility; however, for large NCs, the electronic coupling deteriorates the current, which is mostly carried by two nearest neighboring NCs. In addition, control of inter-NC separation appears to be critical to enhanced carrier mobility. We also anticipate similar size-dependency of carrier mobility in other semiconductor NC arrays. For instance, the crossover diameter of CdSe NC arrays may be larger than 5 nm, which was the largest diameter experimented in ref 2. We envision that a priori determination of the crossover diameter by computations should be highly useful for electronic and optoelectronic device development.

AUTHOR INFORMATION

Corresponding Author

*E-mail: esim@yonsei.ac.kr. Fax: +82-2-364-7050.

Notes

The authors declare no competing financial interest.

ACKNOWLEDGMENTS

This work was supported by the National Research Foundation (NRF) grant funded by the Korea government (2011-0002832, 2011-0003690, and 2010-220-C00017). J.L. thanks the fellowship of the BK 21 program from MOEHRD, Heeyoung Kim for code tutorial, and Min-Cheol Kim for illustration.

REFERENCES

(1) Nozik, A. J.; Beard, M. C.; Luther, J. M.; Law, M.; Ellingson, R. J.; Johnson, J. C. Semiconductor Quantum Dots and Quantum Dot Arrays and Applications of Multiple Exciton Generation to Third-Generation Photovoltaic Solar Cells. *Chem. Rev.* **2010**, *110*, 6873−6890.

(2) Kang, M. S.; Sahu, A.; Norris, D. J.; Frisbie, C. D. Size-Dependent Electrical Transport in CdSe Nanocrystal Thin Films. *Nano Lett.* **2010**, *10*, 3727−3732.

(3) Liu, Y.; Gibbs, M.; Puthussery, J.; Gaik, S.; Ihly, R.; Hillhouse, H. W.; Law, M. Dependence of Carrier Mobility on Nanocrystal Size and Ligand Length in PbSe Nanocrystal Solids. *Nano Lett.* **2010**, *10*, 1960−1969.

(4) *Charge Transport in Disordered Solids*; Baranovski, S., Ed.; Wiley: Chichester, U.K., 2006.

(5) Ashcroft, N. W.; Mermin, N. D. *Solid State Physics*; CBS Publishing Asia: Philadelphia, PA, 1988.

(6) Feynman, R. P.; Hibbs, A. R. *Quantum Mechanics and Path Integrals*; McGraw-Hill: New York, 1965.

(7) Feynman, R. P.; Vernon, F. L. The Theory of a General Quantum System Interacting with a Linear Dissipative System. *J. Ann. Phys.* **1963**, *24*, 118−173.
(8) Makri, N.; Makarov, D. E. Tensor Propagator for Iterative Quantum Time Evolution of Reduced Density-Matrices. 1. Theory. *J. Chem. Phys.* **1995**, *102*, 4600−4610.
(9) Makri, N.; Makarov, D. E. Tensor Propagator for Iterative Quantum Time Evolution of Reduced Density-Matrices. 2. Numerical Methodology. *J. Chem. Phys.* **1995**, *102*, 4611−4618.
(10) Sim, E.; Makri, N. Filtered Propagator Functional for Iterative Dynamics of Quantum Dissipative Systems. *Comput. Phys. Commun.* **1997**, *99*, 335−354.
(11) Sim, E. Quantum Dynamics for a System Coupled to Slow Baths: On-The-Fly Filtered Propagator Method. *J. Chem. Phys.* **2001**, *115*, 4450−4456.
(12) Tang, J.; Kemp, K. W.; Hoogland, S.; Jeong, K. S.; Liu, H.; Levina, L.; Furukawa, M.; Wang, X.; Debnath, R.; Cha, D.; et al. Colloidal-Quantum-Dot Photovoltaics using Atomic-Ligand Passivation. *Nat. Mater.* **2011**, *10*, 765−771.
(13) Caldeira, A. O.; Leggett, A. J. Influence of Dissipation on Quantum Tunneling in Macroscopic Systems. *Phys. Rev. Lett.* **1981**, *46*, 211−214.
(14) Szabo, A.; Zwanzig, R. Reversible Diffusion-Influenced Reactions - Comparison of Theory and Simulation for a Simple-Model. *J. Stat. Phys.* **1991**, *65*, 1057−1083.
(15) Overgaag, K.; Vanmaekelbergh, D.; Liljeroth, P.; Mahieu, G.; Grandidier, B.; Delerue, C.; Allan, G. Electron-Phonon Coupling and Intervalley Splitting Determine the Linewidth of Single-Electron Transport through PbSe Nanocrystals. *J. Chem. Phys.* **2009**, *131*, 224510.
(16) Marcus, R. A. On the Theory of Oxidation-Reduction Reactions Involving Electron Transfer I. *J. Chem. Phys.* **1956**, *24*, 966−978.
(17) Onuchic, J. N.; Wolynes, P. G. Classical and Quantum Pictures of Reaction Dynamics in Condensed Matter: Resonances, Dephasing and all That. *J. Phys. Chem.* **1988**, *92*, 6495−6503.
(18) Sim, E.; Makri, N. Path Integral Simulation of Charge Transfer Dynamics in Photosynthetic Reaction Centers. *J. Phys. Chem. B* **1997**, *101*, 5446−5458.
(19) Makri, N.; Sim, E. J.; Makarov, D. E.; Topaler, M. Long-Time Quantum Simulation of the Primary Charge Separation in Bacterial Photosynthesis. *Proc. Natl. Acad. Sci. U.S.A.* **1996**, *93*, 3926−3931.
(20) Kim, H.; Sim, E. Environmental Effect on the Relative Contribution of the Charge-Transfer Mechanisms within a Short DNA Sequence. *J. Phys. Chem. B* **2006**, *110*, 631−636.
(21) Kim, H.; Sim, E. Distance Dependent Coherence Variation in DNA Charge-Transfer Processes. *J. Phys. Chem. B* **2008**, *112*, 2557−2561.
(22) Kim, H.; Choi, O.; Sim, E. Pathway Analysis on DNA Charge Transfer through Adenine and Guanine Bridges. *J. Phys. Chem. C* **2010**, *114*, 20394−20400.
(23) Kim, H.; Sim, E. Degree of Coherence of Single-Component Molecular Wires: Dependence on Length, Coupling Strength, and Dissipative Medium. *J. Phys. Chem. C* **2009**, *114*, 1312−1316.
(24) Sim, E. Determination of the Electron Transfer Mechanism through Decomposition of the Density Matrix. *J. Phys. Chem. B* **2004**, *108*, 19093−19095.
(25) Sim, E. Effect of the Donor-Bridge Energy Gap on the Electron-Transfer Mechanism in Donor-Bridge-Acceptor Systems. *J. Phys. Chem. B* **2005**, *109*, 11829−11835.
(26) Sim, E.; Kim, H. Analysis of Bridge-Mediated Pathways for Long-Range Charge Transfer Systems. *J. Phys. Chem. B* **2006**, *110*, 16803−16807.
(27) Sim, E.; Kim, H. Characterization of Quantum Dynamically Significant Paths of Bridge-Mediated Charge Transfer Systems. *J. Phys. Chem. B* **2006**, *110*, 13642−13648.
(28) Grove, A. S. *Physics and Technology of Semindoctor Devices*; Wiley: New York, 1967.
(29) Brennan, K. F. A Computer-Aided Approach to Teaching Band Structure Formation. *IEEE Trans. Educ.* **1992**, *35*, 60−68.
(30) Madelung, O. *Semiconductors: Data Handbook*; Springer: New York, 2004.
(31) Tomfohr, J. K.; Sankey, O. F. Complex Band Structure, Decay Lengths, and Fermi Level Alignment in Simple Molecular Electronic Systems. *Phys. Rev. B* **2002**, *65*, 245105.
(32) Talapin, D. V.; Murray, C. B. PbSe Nanocrystal Solids for n- and p-Channel Thin Film Field-Effect Transistors. *Science* **2005**, *310*, 86−89.
(33) Markovich, G.; Collier, C. P.; Henrichs, S. E.; Remacle, F.; Levine, R. D.; Heath, J. R. Architectonic Quantum Dot Solids. *Acc. Chem. Res.* **1999**, *32*, 415−423.
(34) Liu, Y.; Gibbs, M.; Perkins, C. L.; Tolentino, J.; Zarghami, M. H.; Bustamante, J.; Law, M. Robust, Functional Nanocrystal Solids by Infilling with Atomic Layer Deposition. *Nano Lett.* **2011**, *11*, 5349−5355.
(35) Yu, D.; Wang, C.; Guyot-Sionnest, P. n-Type Conducting CdSe Nanocrystal Solids. *Science* **2003**, *300*, 1277−1280.
(36) Kovalenko, M. V.; Scheele, M.; Talapin, D. V. Colloidal Nanocrystals with Molecular Metal Chalcogenide Surface Ligands. *Science* **2009**, *324*, 1417−1420.
(37) Rampi, M. A.; Schueller, O. J. A.; Whitesides, G. M. Alkanethiol Self-Assembled Monolayers as the Dielectric of Capacitors with Nanoscale Thickness. *Appl. Phys. Lett.* **1998**, *72*, 1781−1783.
(38) Liljeroth, P.; Overgaag, K.; Urbieta, A.; Grandidier, B.; Hickey, S. G.; Vanmaekelbergh, D. Variable Orbital Coupling in a Two-Dimensional Quantum-Dot Solid Probed on a Local Scale. *Phys. Rev. Lett.* **2006**, *97*, 096803.
(39) Rozhok, S.; Sun, P.; Piner, R.; Lieberman, M.; Mirkin, C. A. AFM Study of Water Meniscus Formation between an AFM Tip and NaCl Substrate. *J. Phys. Chem. B* **2004**, *108*, 7814−7819.
(40) Leggett, A. J.; Chakravarty, S.; Dorsey, A. T.; Fisher, M. P. A; Garg, A.; Zwerger, W. Dynamics of the Dissipative Two-State System. *Rev. Mod. Phys.* **1987**, *59*, 1−85.
(41) Winterstetter, M. Dissipative Multistate Systems in the Scaling Limit. *Phys. Rev. E* **1999**, *60*, 203−211.
(42) Kang, M. S.; Sahu, A.; Norris, D. J.; Frisbie, C. D. Size- and Temperature-Dependent Charge Transport in PbSe Nanocrystal Thin Films. *Nano Lett.* **2011**, *11*, 3887−3892.
(43) Chandler, R. E.; Houtepen, A. J.; Nelson, J.; Vanmaekelbergh, D. Electron Transport in Quantum Dot Solids: Monte Carlo Simulations of the Effects of Shell Filling, Coulomb Repulsions, and Site Disorder. *Phys. Rev. B* **2007**, *75*, 085325.
(44) Quinn, A. J.; Beecher, P.; Iacopino, D.; Floyd, L.; De Marzi, G.; Shevchenko, E. V.; Weller, H.; Redmond, G. Manipulating the Charging Energy of Nanocrystal Arrays. *Small* **2005**, *1*, 613−618.
(45) Laikhtman, B.; Wolf, E. L. Tunneling Time and Effective Capacitance for Single Electron Tunneling. *Phys. Lett. A* **1989**, *139*, 257−260.
(46) Lane, J. M. D.; Grest, G. S. Spontaneous Asymmetry of Coated Spherical Nanoparticles in Solution and at Liquid-Vapor Interfaces. *Phys. Rev. Lett.* **2010**, *104*, 235501.
(47) Podsiadlo, P.; Krylova, G.; Lee, B.; Critchley, K.; Gosztola, D. J.; Talapin, D. V.; Ashby, P. D.; Shevchenko, E. V. The Role of Order, Nanocrystal Size, and Capping Ligands in the Collective Mechanical Response of Three-Dimensional Nanocrystal Solids. *J. Am. Chem. Soc.* **2010**, *132*, 8953−8960.